ICOLD 75th Annual Meeting
Saint Petersburg, Russia, June 24-29, 2007

Symposium: «Dam Safety Management. Role of State, Private Companies and Public in Designing, Constructing and Operating of Large Dams»

EVALUATION OF CRACK DAMAGES IN CONCRETE THROUGH NONLINEAR DYNAMIC ANALYSES AND SHAKING TABLE TESTS OF LARGE-SCALE MODEL

Takashi SASAKI[1] Yoshikazu YAMAGUCHI[2] Susumu SASAKI[3]
Hiroshi KURAHASHI[4] and Hitoshi YOSHIDA[5]

INTRODUCTION

In view of the As a consequence of frequent large earthquakes that have occurred in Japan in recent years, evaluating the seismic safety of various infrastructures has become an important and urgent issue. In this situation, the Ministry of Land, Infrastructure and Transport of the Japanese Government published the "*Guidelines for Seismic Performance Evaluation of Dams during Large Earthquakes*" in March 2005.

According to the guidelines, numerical analysis considering the tensile fracture of concrete is generally required to evaluate the seismic safety of concrete gravity dams in the event of a large earthquake. The authors have considered the seismic safety of concrete gravity dams by performing non-linear analysis using a smeared crack model (Sasaki, T. *et al*. 2005). However, the applicability of these kinds of analysis methods has been mainly confirmed in a qualitative manner based on a comparison with limited cases of cracking of existing dams during large earthquakes. Therefore, the quantitative evaluation of the analysis method is necessary in order to accurately estimate the cracking phenomena. From this viewpoint, some research activities have been conducted by, for example, Tinawi *et al*. (2000), who performed vibration testing of concrete gravity dam models.

This paper reports on a study of about the fracture of plane concrete by shaking using a pillar-shaped small-scale models and a large-scale model made of low-strength concrete. The test results revealed the influence of tensile cracking of the concrete on the first resonant frequency and the damping ratio of the test model. A numerical analysis was attempted in order to simulate cracking in the test models by finite element analysis using the smeared crack model.

SHAKING TABLE TESTS

Experimental Method

Shape of Test Model

The shapes of the test model arewere shown in Fig. 1. The shapes were decided by taking into account the following conditions: (1) the first resonant frequenciesy of the test models are within the range of the excitation capacity of the shaking table which is planned to be used and (2) it is possible to roughly specify the location where tensile cracking will occur in the models.

In the large-scale model, notches were cut in both ends of the specimen to induce cracking.

In order to control the first resonant frequency, a weight of 100 kg was applied to the top of the small-scale model. The first resonant frequencies of the test models before fracturing were about 30 Hz (small-scale model) and 46Hz (large-scale model).

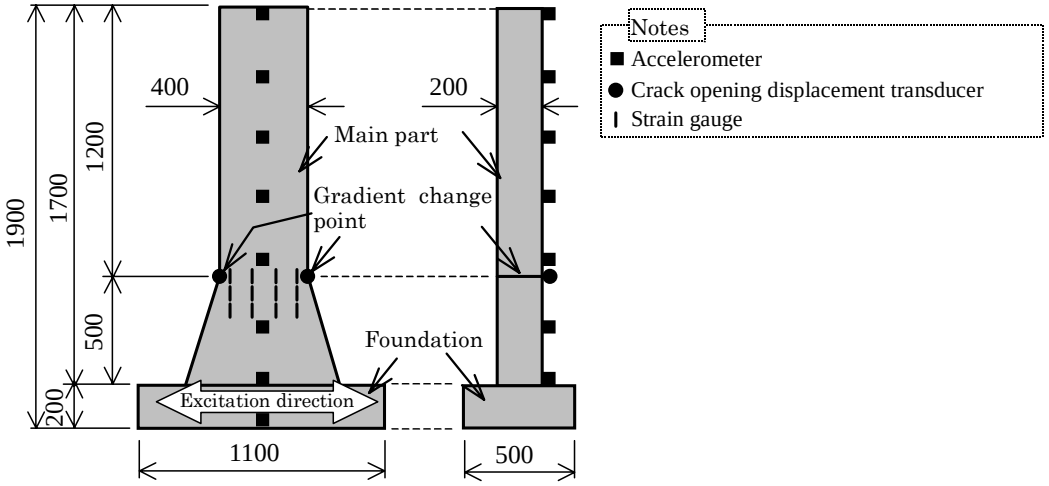

(a) Shape of the small-scale model

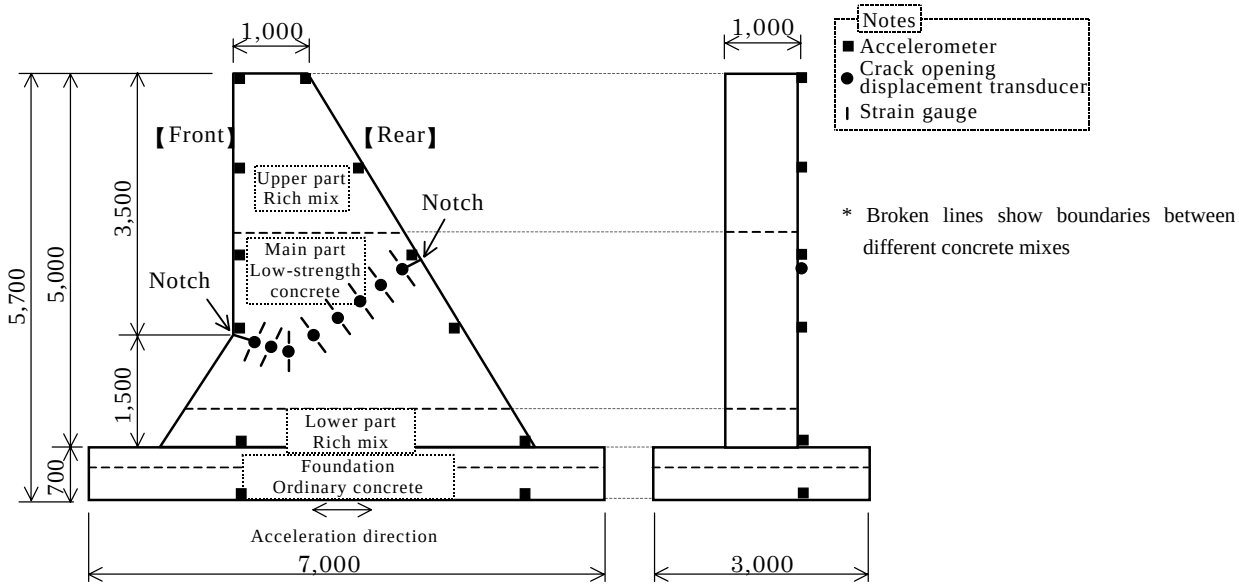

(b) Shape of the large-scale model

Fig. 1 Test model shape (unit: mm)

Material Properties of Test Model

The test models were made from low-strength concrete so that the vibration testing would cause tensile fractures in the models. The fundamental concrete mix proportions and the materials used are shown in Table 1. The maximum aggregate size was set at 20 mm so that the test materials would have a certain degree of fracture energy.

Table 1 Test model materials: Mix proportions and materials

Water : Cement ratio	330 %
Max. aggregate size	20 mm
Cement	Moderate heat Portland cement 67 kg/m^3
Admixture	Limestone powder 433 kg/m^3

Table 2 shows the material properties of low strength concrete obtained by laboratory testing. The test specimens were made with the model for shaking tests, and the laboratory tests were conducted for the same maturity ages with the model for shaking tests.

To obtain the tensile softening properties of the low strength concrete, a wedge penetration type splitting test was performed in compliance with AAC13.1 of RILEM (1994). The specimen was a rectangular parallelepiped with width of 200 mm, height of 1700 mm and thickness of 100mm. Fig. 2 shows the tensile softening curve estimated by a program provided by the Japan Concrete Institute (JCI) based on the back analysis method by using the results of load – crack opening displacement results obtained by the wedge penetration type splitting test (2003).

From the estimated softening curve by the JCI program, approximated bilinear softening curves which are also shown in Fig.2 were obtained so that it is possible to accurately reproduce the results of the wedge penetration type splitting test by FEM numerical analysis.

The fracture energy of the large-scale model became larger than that of the small-scale model because the ordinary strength concrete for the foundation and the rich mix concrete for the lower part of the large-scale model (Fig.1 (b)) might somewhat affected in the low strength concrete of the main part when the mix was changed in the mixing machine.

Table 2 Material properties of the low strength concrete

Property	Small-scale model	Large-scale model
Elastic modulus	5,260 MPa	5,260 MPa
Unit weight	2.3 t/m^3	2.3 t/m^3
Poisson’s ratio	0.15	0.15
Fracture energy	10.5 N/m	23.3 N/m
Softening start stress (for approximated bilinear softening curves)	0.17 MPa	0.38 MPa

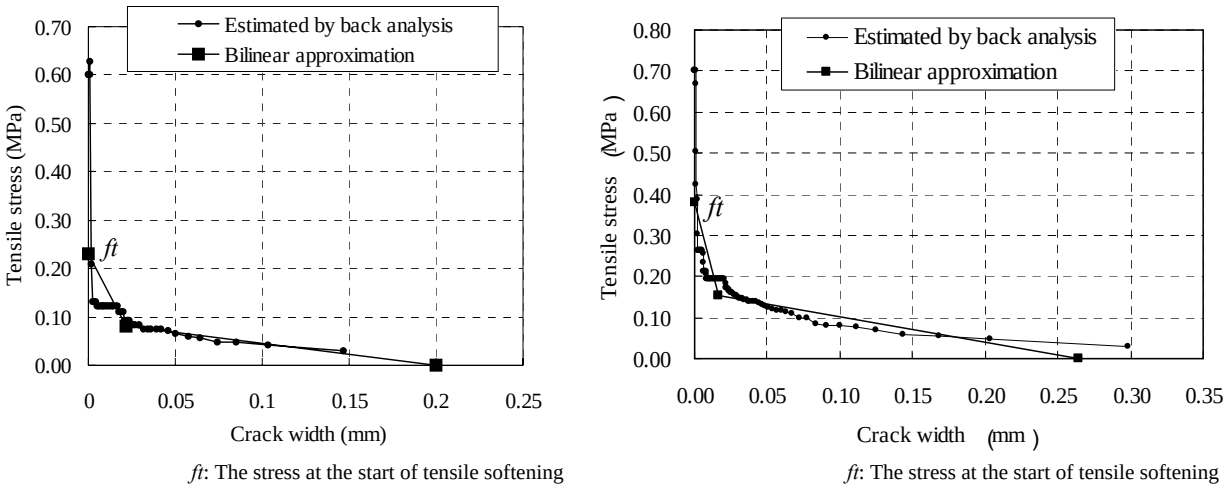

ft: The stress at the start of tensile softening

ft: The stress at the start of tensile softening

(a) Small-scale model (b) Large-scale model

Fig. 2 Tensile softening curve obtained by the wedge penetration type splitting test

Measurement Instruments

On the test models, accelerometers, crack opening displacement transducers and strain gauges were installed. The sampling interval was about 0.001 second (1,000 Hz). The layout of the major instruments is shown in Fig. 1. Visual observation was conducted using a high-speed video camera.

Input Acceleration Wave

The input wave for the small-scale model was set as a sinusoidal wave of 22 Hz. In the case of excitation frequency of 22 Hz, the acceleration response multiplier at the top of the test model is expected to be about 2.5 times. The input wave for the large-scale model was set as a sinusoidal wave of 23 Hz. In the case of excitation frequency of 23 Hz, the acceleration response multiplier at the top of the test model is expected to be about 2.0 times. To make it possible to sufficiently observe the steady response of the test model in one excitation, the excitation time was set to 2 seconds. The amplitude was gradually increased at the beginning period of each excitation. The acceleration amplitude was set to be constant in one excitation, and it was increased step by step with the progress of excitation cases.

Experimental Result of Small-scale Model

Response Acceleration at Top of Test Model

Fig. 3 shows the input acceleration and the response acceleration at the top of the test model in the case with an input acceleration of 300 gal. The response at the top of the test model is shown to be steady-state vibration with identical phase to the input acceleration from 0.5 until about 1.5 seconds, but from about 1.7 seconds, the response acceleration amplitude falls

sharply. This is presumed to be a result of a crack propagating in the test model and passing through it at the 1.7-second point. This was confirmed by the images taken picture data by a high-speed video camera. A phase difference of about 160° was observed between the top response acceleration and the input acceleration after the crack passed through the test model.

Degree of Tensile Fracture

The degree of tensile fracture was defined by Eq. 1 in order to quantitatively evaluate the degree of tensile fracture of the test model. At the time when the degree of tensile fracture was 100%, the tensile softening state had ended and there was a completely opened tensile crack.

$$[\text{Degree of tensile fracture (\%)}]=\Delta d / d \times 100 \quad (1)$$

where, Δd represents the crack tip opening displacement and d represents the displacement when the tensile stress is 0 MPa shown in Fig. 2(a), i.e. 0.2mm.

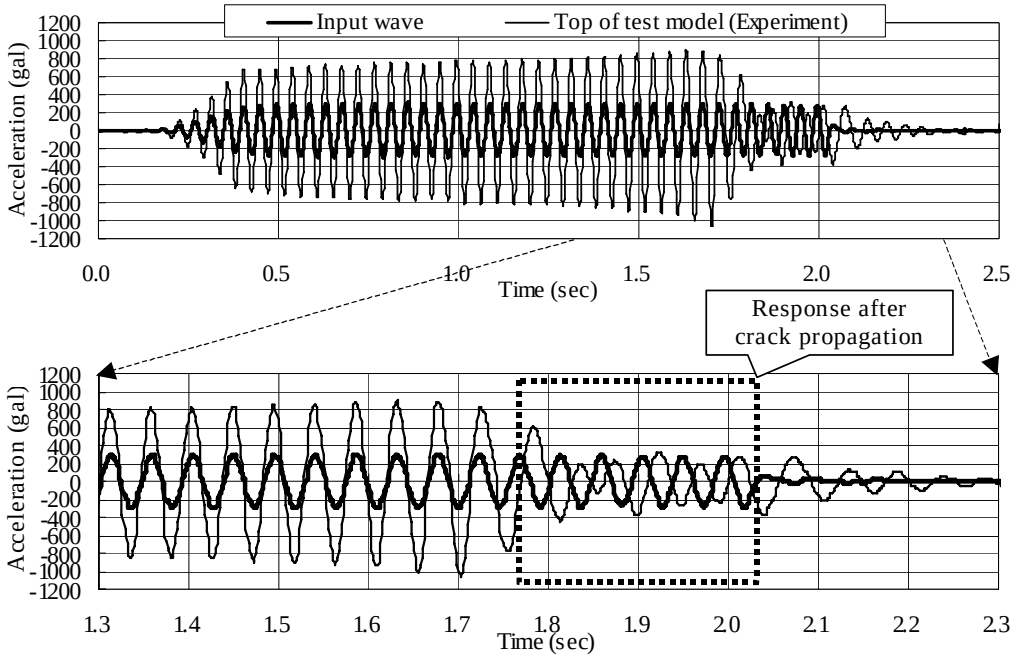

Fig. 3 Response acceleration at top of test model (Input acceleration 300 gal)

Relationship between First Resonant Frequency and Degree of Tensile Fracture

Fig. 4(a) shows the relationship of the degree of tensile fracture with the first resonant frequency calculated based on the response acceleration in the free vibration immediately after termination of the excitation. The open symbol plots in Fig. 4(a) show the analysis results discussed below. This reveals that as the fracture progresses, the first resonant frequency falls.

In the case with input acceleration amplitude of 150 gal, there is almost no decline of the first

resonant frequency from 30 Hz prior to fracturing. On the other hand, in the 300 gal case, the first resonant frequency falls to about 20 Hz, which is lower than the frequency of the input waves (22Hz). This presumably caused the phase difference shown in Fig. 3.

Relationship between Damping Ratio and Degree of Tensile Fracture

Fig. 4(b) shows the relationship of the degree of tensile fracture with the apparent damping ratio obtained based on the response acceleration in the free vibration. The damping ratio was calculated as the average value when m = 1 to 4, and n = 3 based on Eq. 2.

$$\left| y_m / y_{m+n} \right| = \left(e^{2ph/\sqrt{1-h^2}} \right)^n \tag{2}$$

where, y_m and y_{m+n} represent the m and (m+n)th amplitude respectively, and h represents the damping ratio.

Fig. 4(b) reveals that as the degree of tensile fracture increases, the apparent damping ratio rises. In a vibration fracture test of a concrete gravity dam model performed by Tinawi *et al*., it was reported that the occurrence of a crack tended to increase the damping ratio. It is hypothesized that on the fracture surface where the crack occurred, the impact of the re-closing of the crack induces a local fine fracture, which would consumes energy. This would result in an increase in the apparent damping ratio accompanying the appearance of the crack.

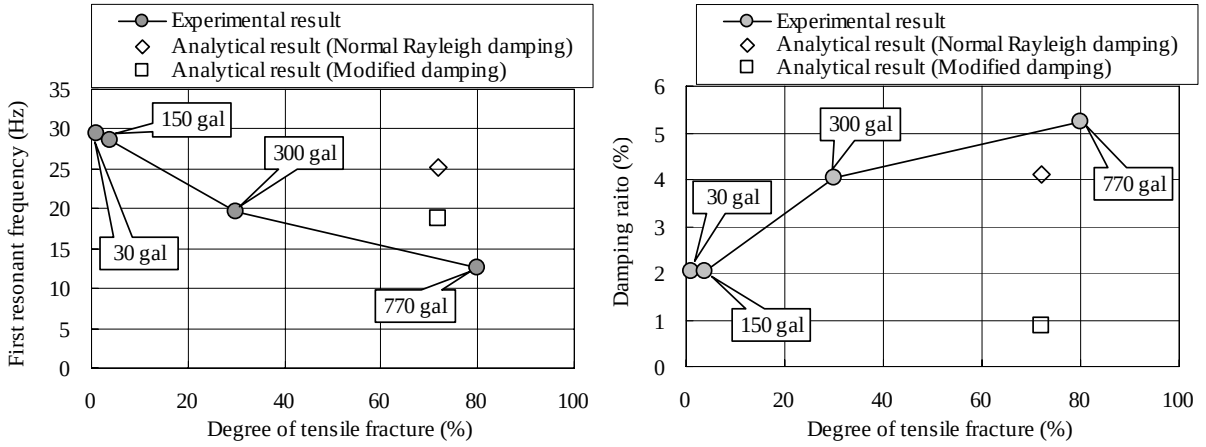

Note: numbers in the figure are the input acceleration amplitude.

(a) First resonant frequency (b) Damping ratio

Fig. 4 First resonant frequency, damping ratio and degree of tensile fracture

Experimental Result of Large-scale Model

Fig. 5 shows the relationship between input acceleration and maximum crack displacement at the front and rear notches. At up to 800 gal input acceleration, crack displacement is proportional to input acceleration in an essentially linear relationship. From about 900 gal,

however, the linear relationship is lost as crack displacement begins to increase more rapidly, with a pronounced spike at 960 gal. Interestingly, the linear relationship begins to disappear in the rear surface cracks at 900 gal, but is preserved up until 960 gal in the front cracks. These observations suggest that significant cracks emerge from the notches on the rear surface at 900 gal, and from the notches on the front surface at 960 gal, with the sudden spike in the crack displacement attributable to the cracks from both ends joining up. Fig. 6 shows sketches of crack displacement after the vibration tests. The response acceleration at the top of the test model, which is not shown in this report, did not change so much, even if the crack passed, unlike the result of the small-scale model test.

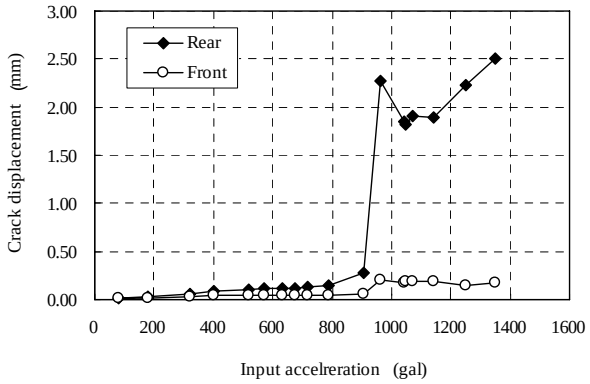

Fig. 5 Maximum crack displacement

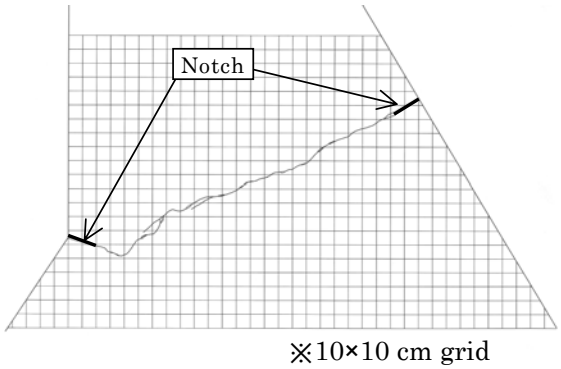

Fig. 6 Crack location in large-scale vibration test

NUMERICAL SIMULATION WITH NON-LINEAR FEM

Numerical Analysis Method

Non-linear finite element analysis based on the smeared crack model was carried out to reproduce the results of the shaking table test. The analysis was two-dimensional hypothesizing the plane stress state, and the concrete tensile softening phenomenon was represented by the bilinear tensile softening curve shown in Fig. 2. The bottom of the test model was considered to be a fixed boundary in FEM analyses. The element models are shown in Fig. 7.

The material properties used for the analysis were set based on the results of laboratory testing, excluding the elastic modulus E, as shown in Table 3. To make the first resonant frequencies of the test models evaluated by the analyses correspond with the values observed in the test, the elastic modulus E for the low strength concrete (main part of the models) waswere set at 6,500 MPa for the small-scale model and 7,700 MPa for the large-scale model, which is a little higher than that evaluated by the material laboratory tests.

The damping matrix in the equation of motion was set by hypothesizing Rayleigh damping at a damping ratio of 2% (small-scale model) and 5%(large-scale model) for the first and second

resonant frequencies. The damping ratio was set so that it would be possible to accurately simulate the linear behavior of the test model before fracturing.

Analytical Results of Small-scale Model

In the numerical analysis, the crack in the test model was almost passed through the test model in the case with an input acceleration amplitude of 340 gal. On the other hand, in the vibration test, the crack passed through at 300 gal. The difference of the accelerations is not so large, and this is presumably due to the fact that the stress at the start of tensile softening *ft* of the bilinearly approximated tensile softening curve in Fig. 2 was about 35% larger than the splitting tensile strength 0.17 MPa of the test material. The analysis results conform closely to the test results in terms of the crack location. Fig. 8 shows the response acceleration at the top of the test model obtained by analysis.

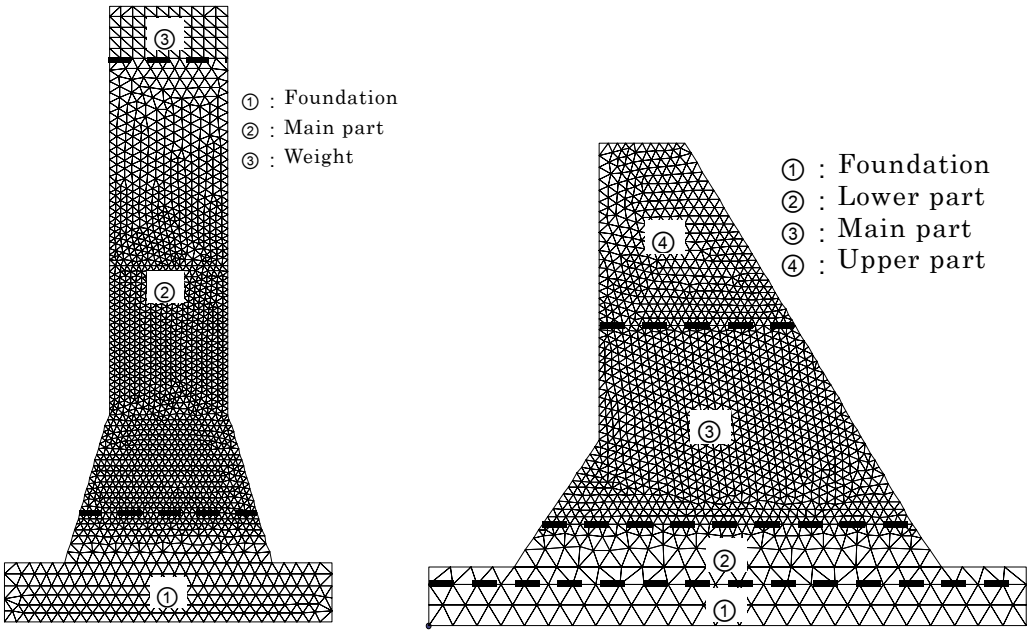

(a) Small-scale model (b) Large-scale model

Fig. 7 Non-linear FE analysis models

Table 3 Material properties for numerical analysis

Material property	Notation	Small-scale model		Large-scale model			
		Main part	Foundation	Main part	Upper part	Lower part	Foundation
Elastic modulus	E (MPa)	6,300	11,000	7,700	19,700	14,800	32,000
Poisson's ratio	ν	0.15	0.15	0.15	0.15	0.15	0.20
Unit weight	ρ (t/m^3)	2.3	2.3	2.3	2.3	2.3	2.3
Damping ratio	h (%)	2	2	5	5	5	5

The following description focuses on the response after 1.0 second when the crack had almost passed through the test model in the analysis result. The phase difference of the top response acceleration to the input wave was calculated to be about only 80°, which it is smaller than that obtained by the shaking test result. Focusing on the reduction of the response acceleration amplitude after the crack passed through, the analysis found no rapid decline of the response acceleration amplitude after the crack passed through. One cause of this phenomenon would be an overevaluation of the viscous damping force in elements in which crack occurred in the analysis. After a crack occurs, the large damping force should not be transmitted passing the crack surface.

In order to appropriately represent the reduction of the viscous damping force on the crack surface, reducing the damping force according to the state of the propagation of the crack was proposed by Kimata *et al*. (2005) and so on. In the present study, non-linear analysis with damping matrix which depends on the state of stiffness matrix with taking consideration of crack was performed. It is similar to methods which were used in the abovementioned researches. The damping matrix was set to be consisted from only stiffness matrix, different from Rayleigh damping. In the following study, we call this damping “modified damping”.

Fig. 9 shows the results of the analysis based on modified damping. Focusing on the response acceleration before cracking, from 0.5 second to about 1.0 second does not show a clear difference between the analysis using normal Rayleigh damping and the analysis with modified damping. This reveals that there are not so large differences between modified damping and Rayleigh damping on the response properties until the crack almost penetrate the test model. Next, focusing on the top response beginning at about 1.0 second when the cracking had propagated reveals large differences between the results in Figs. 8 and 9. Using the method with modified damping, the phase difference between the input acceleration and the response acceleration at the top of the model was about 160°. This result conforms closely to the vibration test result. The analysis also represented the abrupt decline of the response acceleration amplitude after cracking. It seems that modified damping could more appropriately reproduce the response after propagation of the crack.

In Fig. 4, the first resonant frequency and the damping ratio obtained by numerical analyses in the case with an input acceleration of 340 gal are also shown. Degree of tensile fracture of these data was equalized with result of vibration test in case of input acceleration of 300 gal. According to these figures, in the analysis with modified damping, although the first resonant frequency conformed closely to the test result, the damping ratio was much lower than the test result.

There was also a little difference between the absolute values of the response acceleration

amplitude after cracking obtained by analysis and by the vibration test. For these phenomena, it is necessary to study the damping ratio for the overall system according to the degree of progress of cracking (change of the resonant frequency of the overall structure by cracking).

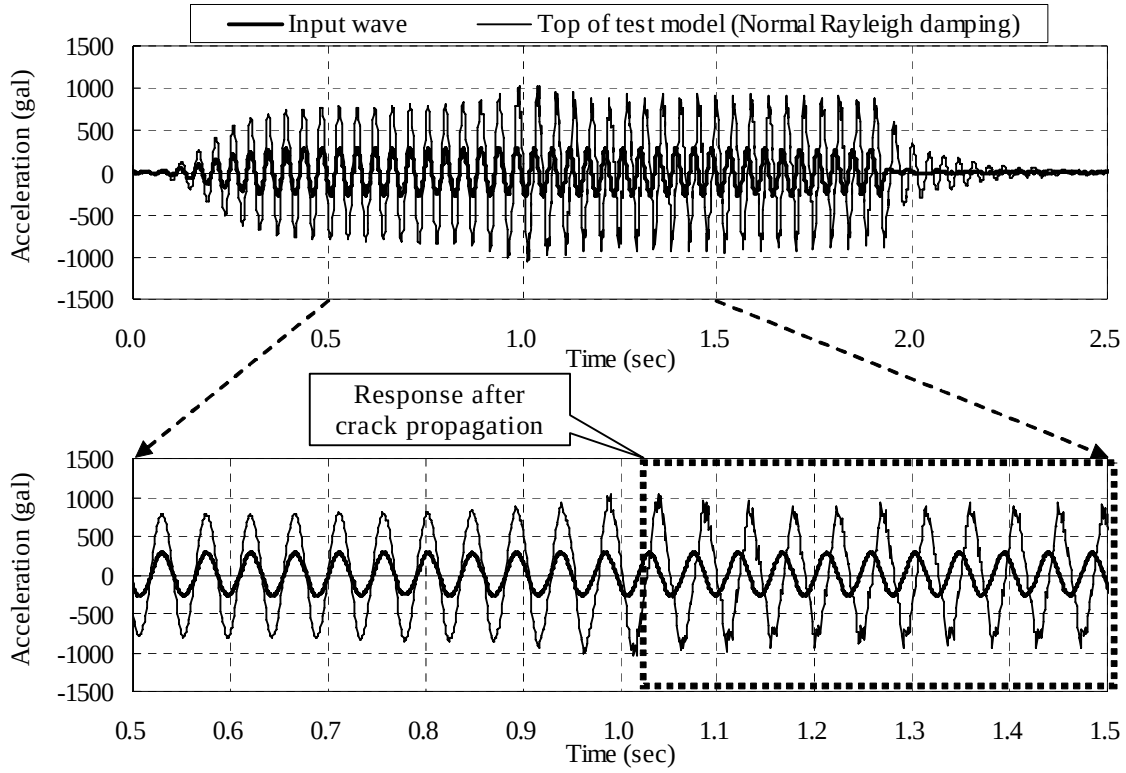

Fig. 8 Acceleration response at top of the small-scale model (normal Rayleigh damping)

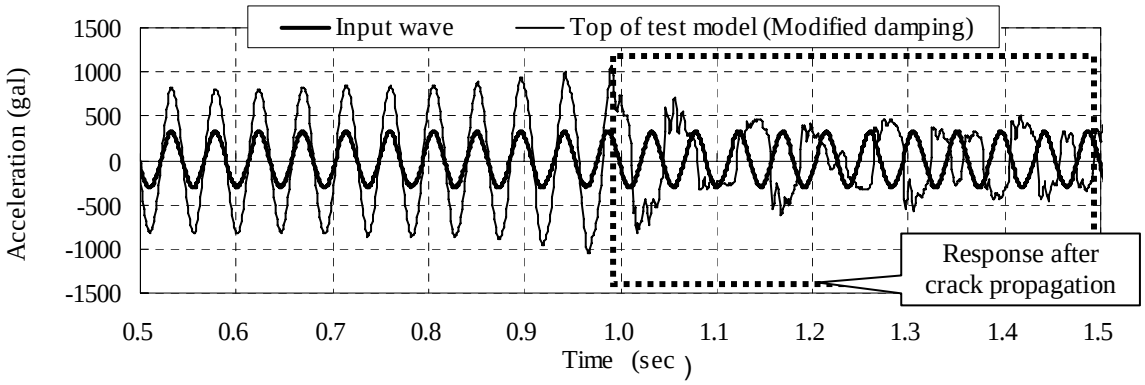

Fig. 9 Acceleration response at top of the small-scale model (modified damping)

Analytical Results of Large-scale Model

The contours of the crack displacement estimated by the dynamic analysis are shown in Fig. 10(a) for the normal Rayleigh damping and in Fig. 10(b) for the modified damping. The amplitude of input acceleration for the numerical analysis was 900 gals. In the test results, the

cracking occurred, but the cracks didn't penetrate through the test model. The location of crack estimated by the analysis using the normal Rayleigh damping is comparative to that by the shaking test.

The crack displacement distribution by the analysis using the modified damping shown in Figure 10(b) is roughly the same as that by the analysis using normal Rayleigh damping shown in Fig. 10(a). Thus, Rayleigh damping is considered acceptable in the dynamic analysis in cases where the cracks do not pass through and where the response characteristics of the structure are relatively constant.

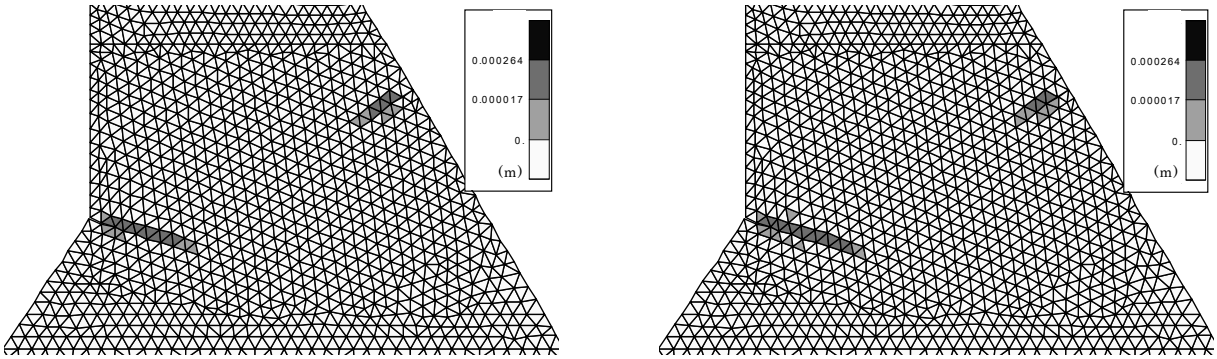

(a) Normal Rayleigh damping (b) Modified damping

Fig. 10 Crack displacement distribution by the analysis for large-scale model

CONCLUSIONS

From considerations based on the results of the shaking test and the non-linear FE analysis based the smeared crack model, the following conclusions were drawn.

- This vibration test confirmed that the progress of tensile fracture was accompanied by a decline of the first resonant frequency and an increase in the apparent damping ratio.
- In the results of the analysis using the tensile softening curve, the location of the crack conformed closely with that in the vibration test results.
- In the case of analysis using Rayleigh damping, the phase and amplitude of the response acceleration after the crack nearly penetrated were significantlymuch different from those in the vibration test results. On the other hand, in the analysis with modified damping which damping matrix depend on the crack extent, the response acceleration at the top of the test model obtained by the analysis and that of the vibration test conformed closely. But, the damping was much underestimated by the analysis using the modified damping.
- For the situation that the crack doesn't penetrate completely and the acceleration response is not so affected by cracks, the smeared crack analysis using normal Rayleigh damping seems to be applicable to estimate the crack location.

A future challenge is to use the results of this research to propose a method of setting material properties including damping ratio for accurately evaluating the seismic safety of a concrete gravity dam.

REFERENCES

Japan Concrete Institute, Method of test for fracture energy of concrete by use of notched beam, *JCI-S-001-2003*, (2003).

Kimata, H., Fujita, Y., Niimi, K., Hoshido, T., Kase, T., Hikawa, N. and Horii, H. Seismic safety of concrete gravity dams based on dynamic crack propagation analysis during large-scale earthquakes, *Proceedings of 73rd Annual Meeting of ICOLD*, (2005).

RILEM AAC13.1, Determination of the specific fracture energy and strain softening of AAC, *RILEM Technical Recommendations for the Testing and Use of Construction Materials*, (1994) 156-158.

River Bureau of Ministry of Land, Infrastructure and Transport, Guidelines for Seismic Performance Evaluation of Dams during Large Earthquakes (2005)

Sasaki, T., Kanenawa, K., Yamaguchi, Y. and Chiba, J. Effect of ground motion level and dam shape on damage in concrete gravity dam during earthquakes, *Proceedings of 73rd Annual Meeting of ICOLD*, (2005).

Tinawi, R., Léger, P., Leclerc. M. and Cipolla, G., Seismic safety of gravity dams: From shake table experiments to numerical analyses, *Journal of Structural Engineering*, (2000) 518-529.

---

[1] Deputy Team Leader, Dam Structure Research Team, Hydraulic Engineering Research Group, Public Works Research Institute (PWRI), Tsukuba-shi, Ibaraki-ken 305-8516 Japan

[2] Team Leader, Dam Structure Research Team, ditto

[3] Researcher, Dam Structure Research Team, ditto

[4] Collaborating Researcher, Dam Structure Research Team, ditto

[5] Group Leader, ditto